# COX-2/sEH dual inhibitor PTUPB attenuates epithelial-mesenchymal transformation of alveolar epithelial cells *via* Nrf2-mediated inhibition of TGF-β1/Smad signaling

**Chen-Yu Zhang**
Central South University
**Xin-Xin Guan**
Central South University
**Zhuo-Hui Song**
Changzhi Medical College
**Hui-Ling Jiang**
Central South University
**Yu-Biao Liu**
Central South University
**Ping Chen**
Central South University
**Jia-Xi Duan**
Central South University
**Yong Zhou** ( zhouyong421@csu.edu.cn )
Central South University https://orcid.org/0000-0002-7348-2376

**Research**

**Keywords:** Pulmonary fibrosis, COX-2/sEH dual inhibitor, Epithelial-mesenchymal transition, Alveolar epithelial cells, Transforming growth factor-β1

**Posted Date:** April 14th, 2022

**DOI:** https://doi.org/10.21203/rs.3.rs-955213/v2

**Version of Record:** A version of this preprint was published at Oxidative Medicine and Cellular Longevity on April 25th, 2022. See the published version at https://doi.org/10.1155/2022/5759626.

# Abstract

**Background:** Arachidonic acid (ARA) metabolites are involved in the pathogenesis of epithelial-mesenchymal transformation (EMT). However, the role of ARA metabolism in the progression of EMT in pulmonary fibrosis (PF) has not been fully elucidated. The purpose of this study was to investigate the role of cytochrome P450 oxidase (CYP)/ soluble epoxide hydrolase (sEH) and cyclooxygenase-2 (COX-2) metabolic disorders of ARA in EMT during PF.

**Methods:** A signal intratracheal injection of bleomycin (BLM) was given to induce PF in C57BL/6J mice. A COX-2/sEH dual inhibitor PTUPB was used to establish the function of CYPs/COX-2 dysregulation to EMT in PF mice. *In vitro* experiments, murine alveolar epithelial cells (MLE12) and human alveolar epithelial cells (A549) were used to explore the roles and mechanisms of PTUPB on transforming growth factor (TGF)-β1-induced EMT.

**Results:** PTUPB treatment reversed the increase of mesenchymal marker molecule α-smooth muscle actin (α-SMA) and the loss of epithelial marker molecule E-Cadherin in lung tissue of PF mice. *In vitro*, COX-2 and sEH protein levels were increased in TGF-β1-treated alveolar epithelial cells (AECs). PTUPB decreased the expression of α-SMA and restored the expression of E-cadherin in TGF-β1-treated AECs, accompanied by reduced migration and collagen synthesis. Moreover, PTUPB attenuates TGF-β1-Smad2/3 pathway activation in AECs *via* Nrf2 antioxidant cascade.

**Conclusion:** PTUPB inhibits EMT in AECs *via* Nrf2-mediated inhibition of the TGF-β1-Smad2/3 pathway, which holds great promise for the clinical treatment of PF.


# 1. Background

Pulmonary fibrosis (PF) is a prototype of chronic, progressive, and fibrotic lung disease. An altered extracellular matrix replaces healthy tissue and alveolar architecture is destroyed, which leads to decreased lung compliance, disrupted gas exchange, and ultimately respiratory failure and death [1]. Although pirfenidone and nintedanib have been authorized by the Food and Drug Administration [2], they only slow down lung function decline in patients with the mild and moderate disease [3]. Therefore, it's urgent to develop an effective treatment for PF.

Epithelial-mesenchymal transition (EMT) is a reversible process in which epithelial cells lose their cellular polarity and obtain migration characteristics through down-regulation of E-cadherin-mediated cell adhesion [4]. EMT is involved in wound healing, fibrosis, embryonic development, and cancer metastasis [5]. Most investigators concur that alveolar type II epithelial cells undergo EMT during PF development [6, 7]. Studies have shown that pulmonary fibroblasts are derived from various routes, of which about one-third are derived from alveolar type II epithelial cells *via* EMT [8]. Transforming growth factor (TGF)-β1 is the most studied and key EMT inducer [9]. TGF-β1 activates its downstream Smad signaling pathway and plays an important role in fibrosis [10]. TGF-β1 binds to its receptor to trigger intracellular signaling and phosphorylates Smad2 and Smad3. Phosphorylated Smad2 and Smad3 are

transported to the nucleus and regulate the transcription of target genes [11]. Consequently, blocking the EMT of alveolar epithelial cells (AECs) might be a promising strategy for the treatment of PF.

Oxidative stress accelerates TGF-β 1-mediated fiber formation by increasing hydrogen peroxide levels, protein damage, DNA degradation, and lipid peroxidation [12]. The transcription factor Nrf2 plays an important role in intracellular antioxidant responses. Activated Nrf2 is transported to the nucleus to promote the transcription of antioxidant enzymes [13]. Nrf2 balances not only oxidative stress but also has negative effects on TGF-β 1-mediated pro-fibrotic signal transduction [14, 15]. Previous studies have shown that Nrf2 plays an important role in preventing lung inflammation and fibrosis [16, 17]. These results indicate that strategies targeting Nrf2 have anti-pulmonary fibrosis potential.

Epoxyeicosatrienoic acids (EETs), leukotrienes (LTs), and prostaglandins (PGs) are derived from arachidonic acid (ARA) with cytochrome P450 oxidase (CYP), lipoxygenase (LOX), and cyclooxygenase (COX) pathways, respectively [18]. ARA metabolites play multiple roles in almost diseases. A previous study found that the knockdown of COX-2 can reduce TGF-β1-induced EMT, indicating that the increased expression of COX-2 is involved in the process of EMT [19]. The up-regulated expression of COX-2 stimulates the production of TGF-β, which is inhibited by NS-398, a selective inhibitor of COX-2 [20, 21]. The activation of a TGF-β1/Smad3 signaling pathway is modulated by an up-regulated expression of COX-2 in benzalkonium chloride-induced subconjunctival fibrosis [10]. In addition, COX-2 has been shown to promote cancer initiation and progression through pleiotropic functions, including EMT induction *via* its predominant product, PGE2, which binds to the cognate receptor EP2 [22]. These studies suggest that the COX-2 metabolism of ARA promotes the process of EMT. ARA metabolism generates EETs *via* the CYP2C/2J metabolic pathway [23]. EETs have various biological activities such as vasodilators, anti-inflammation, and anti-fibrosis [24-28]. We have reported blockade of EETs degradation attenuates murine PF [28]. Besides, EETs inhibit EMT in unilateral ureteral obstruction (UUO) mice by decreasing renal Snail1 and Zinc-finger E-box binding (ZEB) expression [29]. However, EETs are rapidly metabolized by soluble epoxide hydrolase (sEH) [24].

Our previous study suggested that the expressions of sEH and COX-2 are significantly increased in the lungs of PF mice induced by bleomycin (BLM) [30]. A compound that concurrently inhibits both COX-2 and sEH is called 4-(5-phenyl-3-{3-[3-(4-trifluoromethylphenyl)-ureido]-propyl}-pyrazol-1-yl)-benzenesulfonamide (PTUPB), which prevents the release of PGs and increases the blood levels of EETs [31]. PTUPB is more potent in suppressing inflammatory pain and tumor growth than celecoxib, t-AUCB (an inhibitor of sEH), or the combination of celecoxib and t-AUCB [31, 32]. We have shown that PTUPB can alleviate acute lung injury [33], non-alcoholic fatty liver disease [34], and sepsis [35] in mice. What's more, we have found that PTUPB significantly attenuates BLM-induced PF in mice [30]. However, it is not clear whether PTUPB can inhibit EMT. Therefore, the present study aimed to investigate the effect of PTUPB on TGF-β1-mediated pulmonary EMT.

# 2. Materials And Methods

## 2.1 Animal

C57BL/6J mice (adult male, 6-8 weeks) were obtained from Hunan SJA Laboratory Animal Co., Ltd (Hunan, China). Mice were placed in specific pathogen-free conditions for a 12 h day-night cycle. Mice have free access to food and water.

## 2.2 Murine model of PF and treatment

Mice were randomly divided into the control group, PTUPB group, BLM group, and BLM+PTUPB group. For PF induction, mice received an intratracheal injection of BLM (1.5 mg/kg; Nippon Kayaku, Tokyo, Japan) dissolved in 50 μL saline. At the same time, mice in the control and PTUPB groups received 50 μL saline intratracheally. Mice in the PTUPB group and BLM+PTUPB group were subcutaneously injected with PTUPB (5 mg/kg/d) dissolved in PEG400 from day 7 to day 21 after BLM injection. PTUPB was given by Bruce D. Hammock at UC Davis Comprehensive Cancer Center, University of California [31]. PEG400 was subcutaneously injected for the control and BLM groups. Twenty-one days after the BLM injection, mice were sacrificed. All surgeries were performed under anesthesia.

## 2.3 Pulmonary histopathology analysis

The left lung tissue was placed in a tube filled with 4% paraformaldehyde (Servicebio, Wuhan, China, G1101), followed by conventional paraffin embedding. Paraffin-embedded sections were made. Hematoxylin-eosin staining (HE) was used to observe the morphological changes in lung tissue of mice, and Masson staining was used to observe the collagen deposition. The pictures were detected by a microscope (Motic, BA410E, Motic China group CO., LTD. China) equipped with Motic images plus 3.0 (Motic, Motic China group CO., LTD. China). The image was magnified at 200 ×, with a resolution of 683×705, horizontal and vertical resolutions of 96dpi, and a bit depth of 24.

## 2.4 Immunofluorescent staining

The lung tissue sections were dewaxed and hydrated. EDTA buffer was used for antigen repair under high temperature and pressure conditions. 3% $H_2O_2$ was dropped on the sample for 10 min to achieve the purpose of removing endogenous peroxidase (The cells were washed with PBS three times and fixed with 4% paraformaldehyde for 15 minutes. After washing with PBS three times, cells were permeated with 0.3% Triton X-100 for 15 minutes).The sections or cells were incubated in 5% albumin bovine V (BSA; Solarbio, Beijing, China, A8020) for 30 min, and then incubated with α-SMA antibody (1:200; Abcam, Cambridge, MA, USA), E-cadherin antibody (1:200; Cell Signaling Technology, USA), Smad2 antibody (1:200; CST), Smad3 antibody (1:200; Abcam), or Nrf2 antibody (1:300; CST) in 5% BSA overnight at 4°C. The next day, tissue sections were rewarmed at 37 °C for half an hour and then incubated with a FITC-conjugated goat anti-rabbit antibody (1:2000; Abcam). The nuclei were counterstained with DAPI (Invitrogen, Carlsbad, CA, USA). The coverslips were mounted in 90% glycerol in PBS. The fluorescence was detected by a fluorescence microscope (Motic, BA410E, Motic China group CO., LTD. China) equipped with Motic images plus 3.0 (Motic, Motic China group CO., LTD. China). The same field was photographed

for green fluorescence (EX: AT480/30×, BS: AT505DC, EM: AT515lp) and DAPI (EX: AT375/28×, BS: AT415DC, EM: AT460/50m), and then the fields were superimposed using Image J software. The image was magnified at 200 ×, with a resolution is 1920×1440, horizontal and vertical resolution is 72 dpi, and bit depth is 24.

### 2.5 Cell culture and treatment

Cells were cultured in an incubator at 37°C with 5% $CO_2$. The A549 and MLE12 cell lines were purchased from ATCC. The immortalized human alveolar epithelial cells A549 were cultured in RPMI 1640 (Gibco, Grand Island, NY, USA) supplemented with 10% bovine calf serum (Sigma-Aldrich, St. Louis, MO, USA). Murine alveolar epithelial cells MLE-12 cells were cultured in DMEM F-12 (Gibco) supplemented with 2% bovine calf serum (Sigma-Aldrich), 1% penicillin & streptomycin (Solarbio), 1% 100×ITS-G (Insulin-Transferrin-Selenium) (Solarbio), 10 nM hydrocortisone (Solarbio), and 10 nM β-estradiol (Solarbio).

To estimate the effect of PTUPB on TGF-β1 (10 ng/mL)-challenged AECs, a series of concentrations of PTUPB (1 μM) were added 1 h before TGF-β1 stimulation. To evaluate the role of Nrf2 in PTUPB-inhibited EMT, ML385 (Cat. No.: HY-100523, MCE) was added to inhibit Nrf2 1 h before TGF-β1 stimulation.

### 2.6 Scratch wound healing assay

A549 cells were cultured in 12-well plates with 2% bovine calf serum. Assigned areas of the cell surface were scratched with a 200-μL tip and washed with phosphate buffer solution three times [36]. Cells were pre-treated with PTUPB (1 μM) for 1 h, followed by TGF-β1 (10 ng/mL; Novus Biologicals, Littleton, CO, USA). After 48 h of TGF-β1 treatment, the ability of cells to migrate to the scratch area was assessed by measuring the width of the scratch and calculating the difference from the initial width. Photographs were taken with a microscope (Nikon).

### 2.7 Cell proliferation assay

A549 cells were cultured in 96-well plates with 2% bovine calf serum. Cells were pre-treated with PTUPB (1 μM) for 1 h, followed by TGF-β1 (10 ng/mL). After TGF-β1 treatment for 48 h, 10 μL Cell Counting Kit-8 solution (CCK-8, Dojindo Laboratories, Japan) was added to each well and incubated at 37℃ for 1-3 h. The results were detected at 450 nm with a microplate analyzer (Thermo Fisher Scientific, Waltham, MA, USA).

### 2.8 Detection of ROS

ROS in the cells was assessed by kits following the manufacturer's instructions (Cat# ROS: E004, Jiancheng Bioengineering Institute, Nanjing, China).

### 2.9 The quantitative real-time PCR analysis

Total RNA from right middle lung tissue or cells was extracted with RNAiso Plus (Takara, Kusatsu, Japan). Total RNA (1 μg) was reverse transcribed using PrimeScript RT reagent Kit (Takara). Real-time PCR was carried out to detect mRNA expression levels as described in our previous study [37]. Relative expression of genes was computed by the $2^{-\Delta\Delta CT}$ method according to our previous study [38]. The sequence of primers used in this study is shown in Table1.

Table 1. Sequences of specific primers were used in this study.

| Gene | Forward primer (5′-3′) | Reverse primer (5′-3′) |
|---|---|---|
| *m-Snail1* | GTCCAGCTGTAACCATGCCT | TGTCACCAGGACAAATGGGG |
| *m-Zeb1* | GCTGGCAAGACAACGTGAAAG | GCCTCAGGATAAATGACGGC |
| *m-β-actin* | TTCCAGCCTTCCTTCTTG | GGAGCCAGAGCAGTAATC |
| *h-TIMP1* | AGAGTGTCTGCGGATACTTCC | CCAACAGTGTAGGTCTTGGTG |
| *h-MMP9* | TGTACCGCTATGGTTACACTCG | GGCAGGGACAGTTGCTTCT |
| *h-CDH1* | GCTGGACCGAGAGAGTTTCC | CAAAATCCAAGCCCGTGGTG |
| *h-ACTA2* | AAAGCAAGTCCTCCAGCGTT | TTAGTCCCGGGGATAGGCAA |
| *h-Vimentin* | GTCCGCACATTCGAGCAAAG | TGAGGGCTCCTAGCGGTTTA |
| *h-COL1A1* | CCTGGATGCCATCAAAGTCT | AATCCATCGGTCATGCTCTC |
| *h-FN* | AAACCAATTCTTGGAGCAGG | CCATAAAGGGCAACCAAGAG |
| *h-ZEB1* | TTACACCTTTGCATACAGAACCC | TTTACGATTACACCCAGACTGC |
| *h-SNAIL1* | CTAGGCCCTGGCTGCTACAA | CCTGGCACTGGTACTTCTTGA |
| *h-GAPDH* | AATTCCATGGCACCGTCAAG | TGGACTCCACGACGTACTCA |

### 2.10 Western blot

Protein from right lower lung tissue or cells was extracted according to our previous research [30]. A BCA Protein Assay Kit (Thermo Fisher Scientific, USA) was used to quantify protein concentrations. SDS-PAGE gel electrophoresis was performed, and the protein was transferred from the gel to polyvinylidene fluoride membranes (Millipore, Bedford, MA). The membranes were blocked with 5% BSA or skim milk. The membranes were probed with primary antibody against sEH (1:2000; Abcam), COX-2 (1:1000; Servicebio, Wuhan, China), Collagen-I (1:1000; CST), E-cadherin (1:1000; CST), α-SMA (1:2000; SAB, College Park, MA, USA), Smad2 (1:1000; Abcam), Smad3 (1:1000; Abcam), p-Smad2 (1:1000; Abcam), p-Smad3 (1:1000; Abcam), Nrf2 (1:2000; CST), HO-1(1:1000; Abcam), α-Tubulin (1:5000; Servicebio), β-Tubulin (1:5000; Proteintech, Rosemont, IL, USA) or GAPDH (1:2000; Servicebio). The primary antibody was

incubated overnight. Horseradish peroxidase-conjugated secondary antibodies (1:5000; CST) at room temperature for 1 h and enhanced chemiluminescence (Millipore, USA) were applied to detect protein content. Images were captured on the Chemidoc XRS (Bio-Rad) instrument. The bands were quantified using image laboratory analyzer software (Bio-Rad).

### 2.11 Statistical analyses

All data were presented as means ± standard deviation. Statistical analysis was performed using GraphPad Prism 7 (GraphPad Software, Inc, San Diego, CA, USA). Multiple group comparisons were made using a one-way analysis of variance. Tukey's test was used as a post hoc test to make pairwise comparisons. Differences between the two groups were determined by an unpaired *t*-test. All experiments were independently repeated three times. $P < 0.05$ was considered statistically significant.

## 3. Results

### 3.1 PTUPB reduces PF in mice induced by BLM

In this study, a COX-2/sEH dual inhibitor PTUPB (5 mg/kg, s.c. once a day) was employed on the $7^{th}$ day after BLM administration. HE and Masson staining results showed that PTUPB treatment for 14 days also significantly reduced BLM-induced lung histological changes and collagen deposition in the lungs (Figure 1a). PTUPB significantly decreased Collagen I protein (Figure 1b-c) and the expression of tissue inhibitors of metalloproteinase 1 (*Timp1*) mRNA (Figure 1d). At the same time, we found that PTUPB significantly reduced α-SMA expression and restored E-cadherin expression in the lungs (Figure 1e-g). These results suggest that the reduction of PF by PTUPB is related to the reduction of EMT.

### 3.2 COX-2 and sEH expression are increased in TGF-β1-treated AECs

The protein expressions of COX-2 and sEH were detected in TGF-β1-treated A549 and MLE-12 cells. We found that both COX-2 and sEH protein levels were increased in TGF-β1-treated A549 (Figure 2a-c) and MLE-12 cells (Figure 2d-f), indicating that dysregulation of ARA metabolism participates in the development of EMT. These results suggest an important role of COX-2 and sEH dysregulation in the development of EMT.

### 3.3 Prophylactic treatment of PTUPB suppresses the TGF-β1-induced EMT in AECs

Then, we wondered whether PTUPB suppressed the EMT induced by TGF-β1 *in vitro*. We observed that PTUPB alone did not affect the EMT of A549 cells (Figure S1). Further, we found that the treatment with TGF-β1 (10 ng/mL) for 12 h significantly increased the mRNA expression of actin alpha 2 (*ACTA2*) (encoding α-SMA) and *Vimentin*, indicating the occurrence of EMT, which was effectively suppressed by

the pre-treatment with PTUPB in A549 cells (Figure 3a-b). We found that PTUPB (1 μM) was the most effective inhibition concentration. In addition, western blotting results showed that the pre-treatment with PTUPB (1 μM) reduced α-SMA protein expression and restored E-cadherin protein expression induced by TGF-β1 (10 ng/mL) (Figure 3c-h). Collectively, these results provide strong evidence that PTUPB directly suppresses the EMT induced by TGF-β1 in AECs.

### 3.4 Prophylactic treatment of PTUPB inhibits the migration induced by TGF-β1 in A549 cells

We further investigated the effect of PTUPB on TGF-β1-induced cell migration with the scratch wound-healing assay. The results showed that TGF-β1 treatment (10 ng/mL) for 48 h significantly promoted the migration of A549 cells. PTUPB could significantly reduce this effect (Figure 4a-b). In order to confirm that PTUPB inhibits cell migration but not cell proliferation, we further evaluated proliferation with CCK-8. Results showed that this effect didn't attribute to the alteration of cell proliferation (Figure 4c). Taken together, these results indicate that PTUPB suppresses cell migration by inhibiting EMT in AECs.

### 3.5 Prophylactic treatment of PTUPB inhibits the collagen synthesis induced by TGF-β1 in AECs

The collagen synthesis can directly reflect the severity of PF. We found that the gene expression of *COL1A1* and fibronectin (*FN*) was significantly increased in A549 cells stimulated by TGF-β1, which was effectively suppressed by the pre-treatment with PTUPB (Figure 5a-b). TGF-β1 treatment also induced the increase of protein expression of Collagen I in A549 cells and MLE-12 cells (Figure 5c-f). Pre-treatment with PTUPB restored these changes induced by TGF-β1. Altogether, these results indicate that PTUPB inhibits the TGF-β1-induced collagen synthesis in AECs.

### 3.6 Prophylactic treatment of PTUPB disrupts the TGF-β1-Smad2/3 signaling pathway in AECs

To elucidate the mechanism of PTUPB on EMT, we focused on the downstream signaling pathways of TGF-β1, including Smad, MAPK, and PI3K signaling pathways. We found that PTUPB had no significant effect on MAPK and PI3K signaling pathways after TGF-β1 activation (Figure S2). However, after PTUPB pretreatment, TGF-β 1-induced phosphorylation of Smad2 and Smad3 in A549 cells was significantly reduced (Figure 6a-c). Meanwhile, PTUPB was also observed to reduce the phosphorylation of Smad3 in MLE12 cells induced by TGF-β1 (Figure 6d-f). At this time, the total protein of Smad2/3 in MLE12 cells and A549 cells did not change (Figure S3). Furthermore, immunofluorescence was used to observe that PTUPB reduced nuclear translocation of Smad2 and Smad3 in TGF-β1 stimulated MLE12 cells (Figure 6g). Then we found that treatment with PTUPB suppressed the gene expression of the downstream targets of TGF-β1-Smad2/3 signaling, including *ZEB1* and *SNAIL1* (Figure 6h-i). These data indicate that

PTUPB blocks the TGF-β1 signaling pathway through the inhibition of TGF-β1-Smad2/3 activation in AECs.

### 3.7 Prophylactic treatment of PTUPB restores Nrf2-dependent antioxidant pathways in TGF-β1-induced AECs

TGF-β1-induced down-regulation of Nrf2 protein expression and nuclear translocation in MLE12 cells and PTUPB could restore Nrf2 protein expression and nuclear translocation (Figure 7a, b, d). Meanwhile, PTUPB up-regulated ho-1 protein expression downstream of NRF2 (Figure 7a, c). Activation of Nrf2 is beneficial to ROS elimination. As expected, TGF-β1 increased ROS in MLE12 cells, and PTUPB decreased ROS content (Figure 7d). These results suggest that PTUPB could enhance the Nrf2 signaling pathway in AECs.

### 3.8 Inhibition of Nrf2 attenuates PTUPB regulation of TGF-β1/Smad signaling

In MLE12 cells, inhibition of EMT by PTUPB was eliminated by blocking the Nrf2-HO-1 signaling pathway (Figure. 8a-e). PTUPB-mediated nuclear translocations of Smad2 and Smad3 were also reduced with Nrf2 inhibition (Figure. 8h). Similarly, PTUPB-inhibited transcription of Smad2/3-downstream genes was also abolished (Figure 8f-g). These results suggest that activation of Nrf2 plays an important role in the regulatory effects of PTUPB on the TGF-β1/Smad axis.

## 4. Discussion

The transition of AECs into mesenchymal cells has been reported to cause and/or aggravate PF [6]. In this study, the direct effects of PTUPB on the TGF-β1-induced EMT were investigated. We found that PTUPB restored the phenotype changes, reduced the migration ability, and inhibited the collagen synthesis of TGF-β1-stimulated AECs by disrupting the TGF-β1-Smad2/3 pathway. We demonstrate for the first time that PTUPB blocks TGF-β1-induced EMT in AECs by *inhibiting* the TGF-β1-Smad2/3 signaling pathway. We found that PTUPB restored phenotypic changes, reduced migration ability, and inhibited collagen synthesis of TGF-β 1-stimulated AECs. We demonstrated for the first time that PTUPB blocks EMT of AECs by up-regulating Nrf2 and inhibiting the TGF-β1-Smad2/3 signaling pathway.

ARA is one of the most abundant polyunsaturated fatty acids in the body [39]. ARA is involved in a variety of biological processes, such as angiogenesis, cell migration, and apoptosis [40]. It has been found that inhibiting sEH could increase endogenous EETs content and reduce the EMT process [29, 41]. 14,15-EET and its synthetic analog EET-A could decrease the expression of the EMT inducer factors, ZEB1 and Snail1, prevent the decrease of E-cadherin and reduce the expression of mesenchymal/myofibroblast

markers in the UUO model [29]. However, another ARA pathway, COX-2 metabolism, promotes EMT. COX-2 inhibitor-induced EMT reversal with restored E-cadherin expression has been observed in several cancer cells [42, 43]. The COX-2 metabolite PGJ2 induces EMT by up-regulating the expression of snails [44]. It can be seen that different metabolites of ARA play different roles in the process of EMT. We found that the protein expression of sEH and COX-2 increased significantly during the TGF-β1-induced EMT process, manifested by the CYP/COX-2 metabolism disorder in ARA.

Studies have found a common phenomenon in the three metabolic pathways of ARA: inhibition of any one of these pathways may shunt ARA to the other pathway, thereby reducing efficacy and causing adverse reactions [45-47]. For example, NSAIDs may have anti-inflammatory effects by inhibiting COX, but their side effects may increase the risk of stroke and kidney failure [48]. At the same time, selective inhibition of COX-2 reduces the levels of endothelin PGI2 and the platelet aggregator TXA2, which increases the risk of cardiovascular disease [46]. Therefore, the development of bimolecular inhibitors targeting ARA metabolism has become increasingly important. It has long been found that drugs targeting a single molecule can produce other toxicity and drug resistance, while drugs targeting multiple molecules are less likely to develop resistance and have better therapeutic effects [49]. PTUPB is a novel COX-2 and sEH dual inhibitor [31], and we demonstrated that PTUPB could suppress PF [30], acute lung injury [33], non-alcoholic fatty liver disease [34], and sepsis [35]. However, the direct effects of PTUPB on TGF-β1-induced EMT in AECs are unknown. In the present study, PTUPB significantly improved E-cadherin expression, decreased α-SMA expression, and reduced excessive extracellular matrix deposition in BLM-treated mice. TIMPs serve an important role in controlling tissue organization and fibrosis following injury [50]. We found that PTUPB decreased the expression of *Timp1* mRNA in BLM-treated PF mice lung tissue, which may be one of the reasons for decreased collagen synthesis.

Further, *in vitro* EMT models of MLE-12 and A549 cells were induced by exogenous TGF-β1. We found that PTUPB attenuated TGF-β1-induced the acquisition of mesenchymal markers (such as α-SMA), prevented TGF-β1-induced the loss of epithelial markers (such as E-Cadherin), decreased TGF-β1-induced the enhancement of migration ability, reduced TGF-β1-induced the accumulation of collagen synthesis. These results suggest that regulating COX-2/CYP metabolism in AECs alleviates TGF-β1-induced EMT. Our results support the hypothesis that inhibition of COX-2/sEH by PTUPB potently inhibits the progression of EMT. In short, our findings indicate that a COX-2 and sEH dual inhibitor shows pivotal therapeutic potential for EMT.

ROS plays an important role in the process of EMT, and TGF-β 1-induced EMT can be inhibited by interfering with related upstream molecular events or by treating cells with antioxidants to block ROS production [51, 52]. These studies indicate that ROS production is an important signal for EMT initiation. It has been found that restoring intracellular antioxidant signaling pathways can reduce TGF-β1-induced EMT. For example, piperine enhances the Nrf2 antioxidant cascade, reduces TGF-β1-induced ROS accumulation, and eliminates EMT in AML-12 hepatocytes [14]. Our data show that PTUPB restored Nrf2 protein expression and nuclear translocation in TGF-β1-stimulated MLE12 cells, while reducing TGF-β1-induced intracellular ROS levels. In addition, we unveiled that inhibition of Nrf2 abrogated the protective

activity of PTUPB against TGF-β1. Thus, it is reasonable to speculate that targeted activation of Nrf2 is a pivotal contributor to the lung-protective activity of PTUPB.

TGF-β1-activated Smads play an important role in the process of EMT [53]. The combination of activated Smad2 or Smad3 and Smad4 can transcriptionally regulate EMT, while blocking the expression of Smad2 or Smad3 can reduce TGF-β1-induced EMT [54]. TGF-β1 activates TβRI by acting on the receptor complex and directly phosphorylates the C-terminal of Smad2 and Smad3. After phosphorylation, Smad2, Smad3, and Smad4 form trimers, which are transported to the nucleus, bind to DNA-binding transcription factors and cooperatively regulate the transcription of target genes [53]. Our study found that PTUPB significantly reduced TGF-β1-induced phosphorylation of Smad2 and Smad3 in A549. Meanwhile, PTUPB also reduced the phosphorylation level of Smad3 induced by TGF-β1 in MLE12 and tended to decrease the phosphorylation level of Smad2 induced by TGF-β1 in MLE12. From the multiple of Smad2/3 phosphorylation change, we believe that PTUPB mainly inhibited the phosphorylation level of Smad3 in AECs. It was further found that PTUPB decreased the expression of *ZEB1* mRNA and *SNAIL1* mRNA downstream of the TGF-β1-Smad signaling pathway. These data indicate that PTUPB could inhibit activation of the TGF-β1-Smad2/3 pathway, therefore suppressing TGF-β1-induced EMT. Moreover, we also unveiled that in MLE12 cells, inhibition of Nrf2 crippled the regulatory effects of PTUPB on TGF-β1/Smad signaling. This finding suggests that activation of Nrf2 is an important upstream event that explains PTUPB-mediated modulation of intracellular TGF-β1/Smad pathways.

# 5. Conclusion

In summary, our findings demonstrate that the disorder in the COX-2/CYP metabolism of ARA plays a role in TGF-β1-induced EMT. PTUPB inhibits the activation of the TGF-β1-Smad2/3 pathway through the Nrf2 antioxidant cascade, thus inhibiting EMT in AECs (Figure 9). This study might promote the application of PTUPB in PF treatment.

# Abbreviations

Actin alpha 2 (ACTA2); Alveolar epithelial cells (AECs); Arachidonic acid (ARA); Bleomycin (BLM); Cadherin1 (CDH1); Collagen Type I Alpha 1 (COL1A1); Collagen Type I Alpha 3 (COL1A3); Cyclooxygenase (COX); Cytochrome P450 oxidase (CYP); Epithelial-mesenchymal transition (EMT); Epoxyeicosatrienoic acids (EETs); Fibronectin (FN); Heme oxygenase-1 (HO-1); Leukotrienes (LTs); Lipoxygenase (LOX); Nuclear factor erythroid 2-related factor-2 (Nrf2); Prostaglandins (PGs); Pulmonary fibrosis (PF); Reactive oxygen species (ROS); Soluble epoxide hydrolase (sEH); Transforming growth factor (TGF)-β1; Tissue inhibitor of metalloproteinase1 (TIMP1); Unilateral ureteral obstruction (UUO); α-smooth muscle actin (α-SMA); 4-(5-phenyl-3-{3-[3-(4-trifluoromethylphenyl)-ureido]-propyl}-pyrazol-1-yl)-benzenesulfonamide (PTUPB); Zinc-finger E-box binding (ZEB).

# Declarations

## Ethics approval and consent to participate

All animal experiments were approved by the Ethics Committee of the School of Basic Medical Science, Central South University (No. 2019-0901, Changsha, China).

## Consent for publication

Not applicable.

## Availability of data and materials

The datasets generated during and/or analyzed during the current study are available from the corresponding author on reasonable request.

## Competing interests

The authors declared no conflict of interests.


## Funding

This study was supported by the National Natural Science Foundation of China (91949110), High School Innovation Fund of Hunan province (18K009), Scientific and technological innovation projects of colleges and universities in Shanxi Province (2019L0694), and Fundamental Research Funds for the Central Universities of Central South University (2021zzts0314).


Author Contributions

Y.Z. and J.X.D. conceived and designed the experiments. C.Y.Z., X.X.G., and H.L.J. performed the experiments. C.Y.Z., Y.B.L., and Z.H.S. analyzed the data. Y.Z., P.C., and J.X.D. contributed reagents/materials/analysis tools. C.Y.Z. and Y.Z. wrote the paper. Y.Z. and J.X.D. critically reviewed the manuscript.


Acknowledgments

The authors would like to thank all the institutions and researchers who contributed to this study.

### Authors declare

The preprint has previously been published [55].

# References

1. Richeldi L, Collard HR, Jones MG: Idiopathic pulmonary fibrosis. *Lancet* 2017, 389(10082):1941-1952.

2. Lehtonen ST, Veijola A, Karvonen H, Lappi-Blanco E, Sormunen R, Korpela S, Zagai U, Skold MC, Kaarteenaho R: Pirfenidone and nintedanib modulate properties of fibroblasts and myofibroblasts in idiopathic pulmonary fibrosis. *Respir Res* 2016, 17:14.

3. Mora AL, Rojas M, Pardo A, Selman M: Emerging therapies for idiopathic pulmonary fibrosis, a progressive age-related disease. *Nat Rev Drug Discov* 2017, 16(11):755-772.

4. Yao L, Conforti F, Hill C, Bell J, Drawater L, Li J, Liu D, Xiong H, Alzetani A, Chee SJ *et al*: Paracrine signalling during ZEB1-mediated epithelial-mesenchymal transition augments local myofibroblast differentiation in lung fibrosis. *Cell Death Differ* 2019, 26(5):943-957.

5. Nieto MA, Huang RY, Jackson RA, Thiery JP: Emt: 2016. *Cell* 2016, 166(1):21-45.

6. Zhou L, Gao R, Hong H, Li X, Yang J, Shen W, Wang Z, Yang J: Emodin inhibiting neutrophil elastase-induced epithelial-mesenchymal transition through Notch1 signalling in alveolar epithelial cells. *J Cell Mol Med* 2020, 24(20):11998-12007.

7. Qu J, Zhang Z, Zhang P, Zheng C, Zhou W, Cui W, Xu L, Gao J: Downregulation of HMGB1 is required for the protective role of Nrf2 in EMT-mediated PF. *J Cell Physiol* 2019, 234(6):8862-8872.

8. Tanjore H, Xu XC, Polosukhin VV, Degryse AL, Li B, Han W, Sherrill TP, Plieth D, Neilson EG, Blackwell TS *et al*: Contribution of epithelial-derived fibroblasts to bleomycin-induced lung fibrosis. *Am J Respir Crit Care Med* 2009, 180(7):657-665.

9. Su J, Morgani SM, David CJ, Wang Q, Er EE, Huang YH, Basnet H, Zou Y, Shu W, Soni RK *et al*: TGF-beta orchestrates fibrogenic and developmental EMTs via the RAS effector RREB1. *Nature* 2020, 577(7791):566-571.

10. Huang C, Wang H, Pan J, Zhou D, Chen W, Li W, Chen Y, Liu Z: Benzalkonium chloride induces subconjunctival fibrosis through the COX-2-modulated activation of a TGF-beta1/Smad3 signaling pathway. *Invest Ophthalmol Vis Sci* 2014, 55(12):8111-8122.

11. Gwon MG, An HJ, Kim JY, Kim WH, Gu H, Kim HJ, Leem J, Jung HJ, Park KK: Anti-fibrotic effects of synthetic TGF-beta1 and Smad oligodeoxynucleotide on kidney fibrosis in vivo and in vitro through inhibition of both epithelial dedifferentiation and endothelial-mesenchymal transitions. *FASEB J* 2020, 34(1):333-349.

12. Dendooven A, Ishola DA, Jr., Nguyen TQ, Van der Giezen DM, Kok RJ, Goldschmeding R, Joles JA: Oxidative stress in obstructive nephropathy. *Int J Exp Pathol* 2011, 92(3):202-210.

13. Kikuchi N, Ishii Y, Morishima Y, Yageta Y, Haraguchi N, Itoh K, Yamamoto M, Hizawa N: Nrf2 protects against pulmonary fibrosis by regulating the lung oxidant level and Th1/Th2 balance. *Respir Res* 2010, 11:31.

14. Shu G, Yusuf A, Dai C, Sun H, Deng X: Piperine inhibits AML-12 hepatocyte EMT and LX-2 HSC activation and alleviates mouse liver fibrosis provoked by CCl4: roles in the activation of the Nrf2 cascade and subsequent suppression of the TGF-beta1/Smad axis. *Food Funct* 2021, 12(22):11686-11703.

15. Aminzadeh MA, Nicholas SB, Norris KC, Vaziri ND: Role of impaired Nrf2 activation in the pathogenesis of oxidative stress and inflammation in chronic tubulo-interstitial nephropathy. *Nephrol Dial Transplant* 2013, 28(8):2038-2045.

16. Han YY, Gu X, Yang CY, Ji HM, Lan YJ, Bi YQ, Si R, Qu J, Cheng MH, Gao J: Protective effect of dimethyl itaconate against fibroblast-myofibroblast differentiation during pulmonary fibrosis by inhibiting TXNIP. *J Cell Physiol* 2021, 236(11):7734-7744.

17. Zhao J, Shi J, Shan Y, Yu M, Zhu X, Zhu Y, Liu L, Sheng M: Asiaticoside inhibits TGF-beta1-induced mesothelial-mesenchymal transition and oxidative stress via the Nrf2/HO-1 signaling pathway in the human peritoneal mesothelial cell line HMrSV5. *Cell Mol Biol Lett* 2020, 25:33.

18. Hanna VS, Hafez EAA: Synopsis of arachidonic acid metabolism: A review. *J Adv Res* 2018, 11:23-32.

19. Li F, Sun Y, Jia J, Yang C, Tang X, Jin B, Wang K, Guo P, Ma Z, Chen Y *et al*: Silibinin attenuates TGFbeta1induced migration and invasion via EMT suppression and is associated with COX2 downregulation in bladder transitional cell carcinoma. *Oncol Rep* 2018, 40(6):3543-3550.

20. Tsujii M, Kawano S, Tsuji S, Sawaoka H, Hori M, DuBois RN: Cyclooxygenase regulates angiogenesis induced by colon cancer cells. *Cell* 1998, 93(5):705-716.

21. LaPointe MC, Mendez M, Leung A, Tao Z, Yang XP: Inhibition of cyclooxygenase-2 improves cardiac function after myocardial infarction in the mouse. *Am J Physiol Heart Circ Physiol* 2004, 286(4):H1416-1424.

22. Watanabe Y, Imanishi Y, Ozawa H, Sakamoto K, Fujii R, Shigetomi S, Habu N, Otsuka K, Sato Y, Sekimizu M *et al*: Selective EP2 and Cox-2 inhibition suppresses cell migration by reversing epithelial-to-

mesenchymal transition and Cox-2 overexpression and E-cadherin downregulation are implicated in neck metastasis of hypopharyngeal cancer. *Am J Transl Res* 2020, 12(3):1096-1113.

23. Imig JD: Epoxides and soluble epoxide hydrolase in cardiovascular physiology. *Physiol Rev* 2012, 92(1):101-130.

24. Zarriello S, Tuazon JP, Corey S, Schimmel S, Rajani M, Gorsky A, Incontri D, Hammock BD, Borlongan CV: Humble beginnings with big goals: Small molecule soluble epoxide hydrolase inhibitors for treating CNS disorders. *Prog Neurobiol* 2019, 172:23-39.

25. He Z, Yang Y, Wen Z, Chen C, Xu X, Zhu Y, Wang Y, Wang DW: CYP2J2 metabolites, epoxyeicosatrienoic acids, attenuate Ang II-induced cardiac fibrotic response by targeting Galpha12/13. *J Lipid Res* 2017, 58(7):1338-1353.

26. Zhou Y, Liu T, Duan JX, Li P, Sun GY, Liu YP, Zhang J, Dong L, Lee KSS, Hammock BD *et al*: Soluble Epoxide Hydrolase Inhibitor Attenuates Lipopolysaccharide-Induced Acute Lung Injury and Improves Survival in Mice. *Shock* 2017, 47(5):638-645.

27. Luo XQ, Duan JX, Yang HH, Zhang CY, Sun CC, Guan XX, Xiong JB, Zu C, Tao JH, Zhou Y *et al*: Epoxyeicosatrienoic acids inhibit the activation of NLRP3 inflammasome in murine macrophages. *J Cell Physiol* 2020, 235(12):9910-9921.

28. Zhou Y, Yang J, Sun GY, Liu T, Duan JX, Zhou HF, Lee KS, Hammock BD, Fang X, Jiang JX *et al*: Soluble epoxide hydrolase inhibitor 1-trifluoromethoxyphenyl-3- (1-propionylpiperidin-4-yl) urea attenuates bleomycin-induced pulmonary fibrosis in mice. *Cell Tissue Res* 2016, 363(2):399-409.

29. Skibba M, Hye Khan MA, Kolb LL, Yeboah MM, Falck JR, Amaradhi R, Imig JD: Epoxyeicosatrienoic Acid Analog Decreases Renal Fibrosis by Reducing Epithelial-to-Mesenchymal Transition. *Front Pharmacol* 2017, 8:406.

30. Zhang CY, Duan JX, Yang HH, Sun CC, Zhong WJ, Tao JH, Guan XX, Jiang HL, Hammock BD, Hwang SH *et al*: COX-2/sEH dual inhibitor PTUPB alleviates bleomycin-induced pulmonary fibrosis in mice via inhibiting senescence. *FEBS J* 2020, 287(8):1666-1680.

31. Hwang SH, Wagner KM, Morisseau C, Liu JY, Dong H, Wecksler AT, Hammock BD: Synthesis and structure-activity relationship studies of urea-containing pyrazoles as dual inhibitors of cyclooxygenase-2 and soluble epoxide hydrolase. *J Med Chem* 2011, 54(8):3037-3050.

32. Zhang G, Panigrahy D, Hwang SH, Yang J, Mahakian LM, Wettersten HI, Liu JY, Wang Y, Ingham ES, Tam S *et al*: Dual inhibition of cyclooxygenase-2 and soluble epoxide hydrolase synergistically suppresses primary tumor growth and metastasis. *Proc Natl Acad Sci U S A* 2014, 111(30):11127-11132.

33. Yang HH, Duan JX, Liu SK, Xiong JB, Guan XX, Zhong WJ, Sun CC, Zhang CY, Luo XQ, Zhang YF *et al*: A COX-2/sEH dual inhibitor PTUPB alleviates lipopolysaccharide-induced acute lung injury in mice by

inhibiting NLRP3 inflammasome activation. *Theranostics* 2020, 10(11):4749-4761.

34. Sun CC, Zhang CY, Duan JX, Guan XX, Yang HH, Jiang HL, Hammock BD, Hwang SH, Zhou Y, Guan CX *et al*: PTUPB ameliorates high-fat diet-induced non-alcoholic fatty liver disease via inhibiting NLRP3 inflammasome activation in mice. *Biochem Biophys Res Commun* 2020, 523(4):1020-1026.

35. Zhang YF, Sun CC, Duan JX, Yang HH, Zhang CY, Xiong JB, Zhong WJ, Zu C, Guan XX, Jiang HL *et al*: A COX-2/sEH dual inhibitor PTUPB ameliorates cecal ligation and puncture-induced sepsis in mice via anti-inflammation and anti-oxidative stress. *Biomed Pharmacother* 2020, 126:109907.

36. Shao M, Wen ZB, Yang HH, Zhang CY, Xiong JB, Guan XX, Zhong WJ, Jiang HL, Sun CC, Luo XQ *et al*: Exogenous angiotensin (1-7) directly inhibits epithelial-mesenchymal transformation induced by transforming growth factor-beta1 in alveolar epithelial cells. *Biomed Pharmacother* 2019, 117:109193.

37. Zhong WJ, Yang HH, Guan XX, Xiong JB, Sun CC, Zhang CY, Luo XQ, Zhang YF, Zhang J, Duan JX *et al*: Inhibition of glycolysis alleviates lipopolysaccharide-induced acute lung injury in a mouse model. *J Cell Physiol* 2019, 234(4):4641-4654.

38. Zhong WJ, Duan JX, Liu T, Yang HH, Guan XX, Zhang CY, Yang JT, Xiong JB, Zhou Y, Guan CX *et al*: Activation of NLRP3 inflammasome up-regulates TREM-1 expression in murine macrophages via HMGB1 and IL-18. *Int Immunopharmacol* 2020, 89(Pt A):107045.

39. Martin SA, Brash AR, Murphy RC: The discovery and early structural studies of arachidonic acid. *J Lipid Res* 2016, 57(7):1126-1132.

40. Martinez-Orozco R, Navarro-Tito N, Soto-Guzman A, Castro-Sanchez L, Perez Salazar E: Arachidonic acid promotes epithelial-to-mesenchymal-like transition in mammary epithelial cells MCF10A. *Eur J Cell Biol* 2010, 89(6):476-488.

41. Yang SH, Kim YC, An JN, Kim JH, Lee J, Lee HY, Cho JY, Paik JH, Oh YK, Lim CS *et al*: Active maintenance of endothelial cells prevents kidney fibrosis. *Kidney Res Clin Pract* 2017, 36(4):329-341.

42. Bocca C, Ievolella M, Autelli R, Motta M, Mosso L, Torchio B, Bozzo F, Cannito S, Paternostro C, Colombatto S *et al*: Expression of Cox-2 in human breast cancer cells as a critical determinant of epithelial-to-mesenchymal transition and invasiveness. *Expert Opin Ther Targets* 2014, 18(2):121-135.

43. St John MA, Dohadwala M, Luo J, Wang G, Lee G, Shih H, Heinrich E, Krysan K, Walser T, Hazra S *et al*: Proinflammatory mediators upregulate snail in head and neck squamous cell carcinoma. *Clin Cancer Res* 2009, 15(19):6018-6027.

44. Choi J, Suh JY, Kim DH, Na HK, Surh YJ: 15-Deoxy-Delta(12,14)-prostaglandin J2 Induces Epithelial-to-mesenchymal Transition in Human Breast Cancer Cells and Promotes Fibroblast Activation. *J Cancer Prev* 2020, 25(3):152-163.

45. Liu Y, Tang H, Liu X, Chen H, Feng N, Zhang J, Wang C, Qiu M, Yang J, Zhou X: Frontline Science: Reprogramming COX-2, 5-LOX, and CYP4A-mediated arachidonic acid metabolism in macrophages by salidroside alleviates gouty arthritis. *J Leukoc Biol* 2019, 105(1):11-24.

46. P JJ, Manju SL, Ethiraj KR, Elias G: Safer anti-inflammatory therapy through dual COX-2/5-LOX inhibitors: A structure-based approach. *Eur J Pharm Sci* 2018, 121:356-381.

47. Kim HS, Kim SK, Kang KW: Differential Effects of sEH Inhibitors on the Proliferation and Migration of Vascular Smooth Muscle Cells. *Int J Mol Sci* 2017, 18(12).

48. Cooper C, Chapurlat R, Al-Daghri N, Herrero-Beaumont G, Bruyere O, Rannou F, Roth R, Uebelhart D, Reginster JY: Safety of Oral Non-Selective Non-Steroidal Anti-Inflammatory Drugs in Osteoarthritis: What Does the Literature Say? *Drugs Aging* 2019, 36(Suppl 1):15-24.

49. Zimmermann GR, Lehar J, Keith CT: Multi-target therapeutics: when the whole is greater than the sum of the parts. *Drug Discov Today* 2007, 12(1-2):34-42.

50. Zuo WL, Zhao JM, Huang JX, Zhou W, Lei ZH, Huang YM, Huang YF, Li HG: Effect of bosentan is correlated with MMP-9/TIMP-1 ratio in bleomycin-induced pulmonary fibrosis. *Biomed Rep* 2017, 6(2):201-205.

51. Ma M, Shi F, Zhai R, Wang H, Li K, Xu C, Yao W, Zhou F: TGF-beta promote epithelial-mesenchymal transition via NF-kappaB/NOX4/ROS signal pathway in lung cancer cells. *Mol Biol Rep* 2021, 48(3):2365-2375.

52. Su X, Yang Y, Guo C, Zhang R, Sun S, Wang Y, Qiao Q, Fu Y, Pang Q: NOX4-Derived ROS Mediates TGF-beta1-Induced Metabolic Reprogramming during Epithelial-Mesenchymal Transition through the PI3K/AKT/HIF-1alpha Pathway in Glioblastoma. *Oxid Med Cell Longev* 2021, 2021:5549047.

53. Xu J, Lamouille S, Derynck R: TGF-beta-induced epithelial to mesenchymal transition. *Cell Res* 2009, 19(2):156-172.

54. Valcourt U, Kowanetz M, Niimi H, Heldin CH, Moustakas A: TGF-beta and the Smad signaling pathway support transcriptomic reprogramming during epithelial-mesenchymal cell transition. *Mol Biol Cell* 2005, 16(4):1987-2002.

55. Chen-Yu Z, Xin-Xin G, Zhuo-Hui S, Hui-Ling J, Yu-Biao L, Ping C, Jia-Xi D, Yong Z: *Research Square* 2021.

# Figures

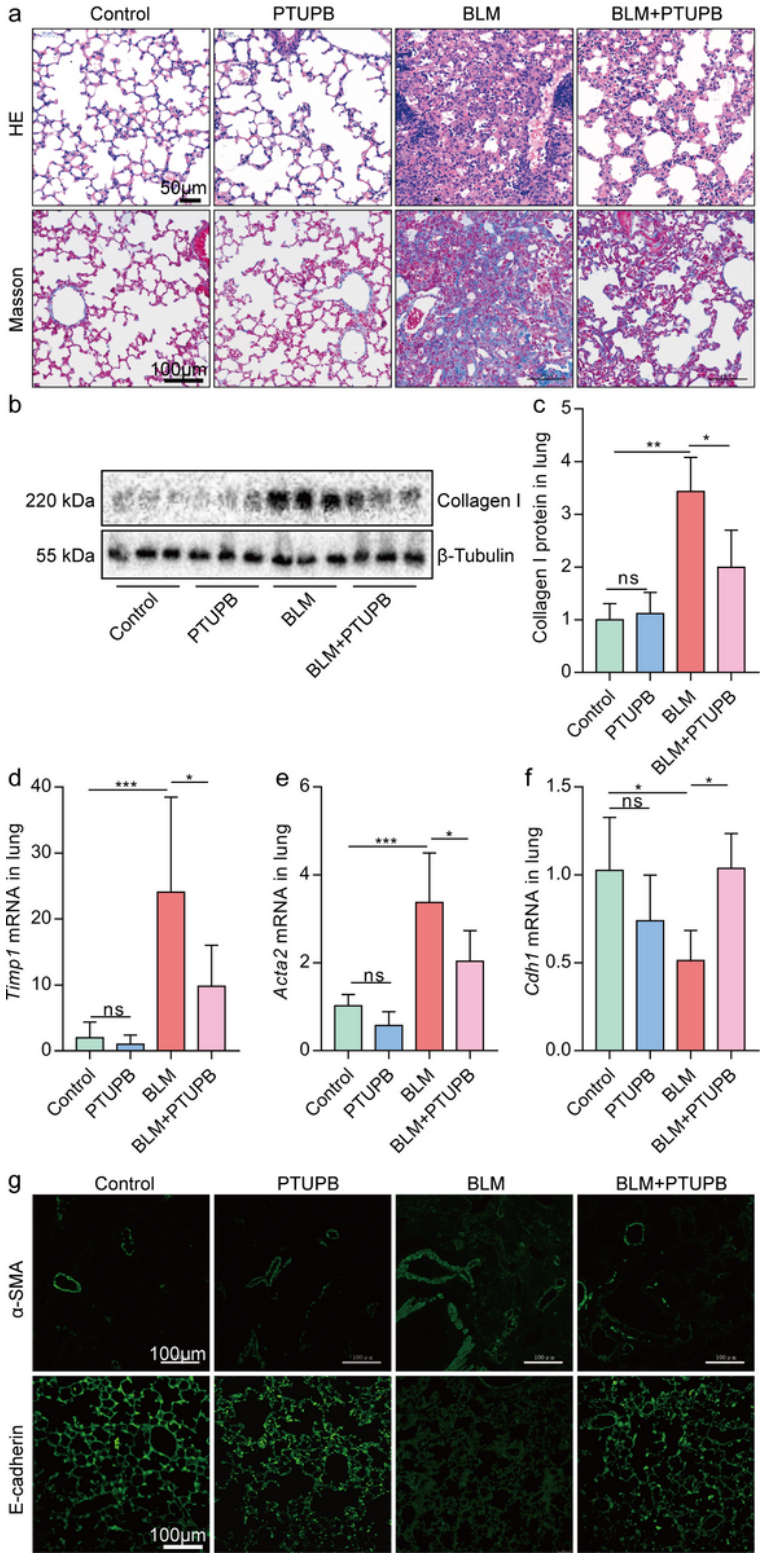


## Figure 1

PTUPB reduces pulmonary fibrosis in mice induced by BLM. Mice received an intratracheal injection of BLM (1.5 mg/kg). Twenty-one days later, HE and Masson staining were employed to evaluate the pulmonary morphology changes and collagen disposition (a; HE staining: bar=50 μm; Masson staining: bar=100 μm). The Collagen I protein expression was detected by western blotting (b-c, n=6). The mRNA expressions of Timp1, Acta2, and Cdh1; were detected by real-time PCR (d-f, n=5-6). The deposition of α-

SMA and E-cadherin were detected by immunofluorescence (e, bar=100 μm). Data are expressed as the mean ± SD. Differences among multiple groups were performed using ANOVA. Tukey's test was used as a post hoc test to make pairwise comparisons. *P < 0.05, **P < 0.01, and ***P < 0.001.

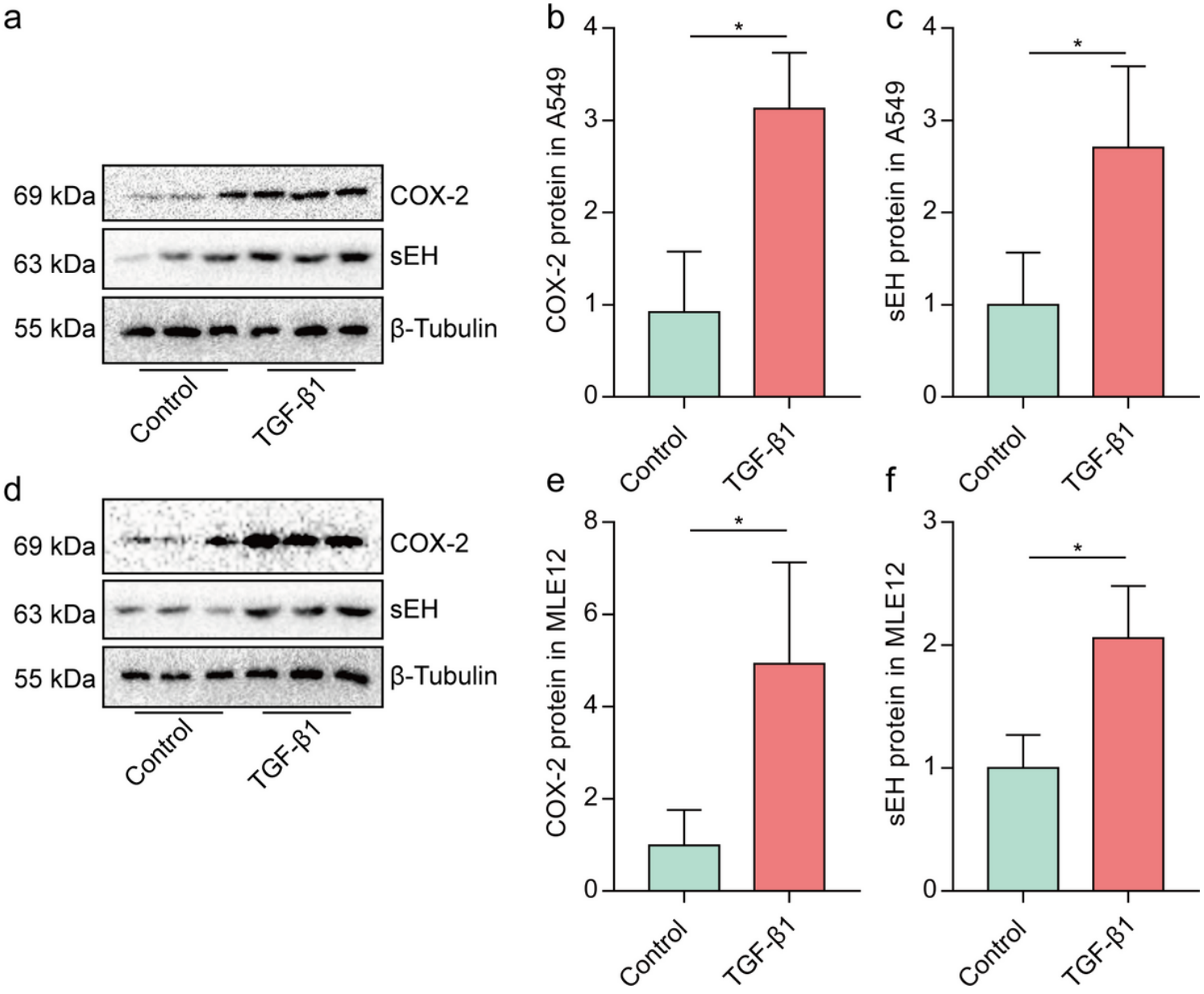


## Figure 2

COX-2 and sEH expression are increased in TGF-β1-treated AECs. COX-2 and sEH protein expressions in A549 cells (a-c) and MLE-12 cells (d-f) were detected using western blot (n=3). Data shown are from a representative experiment with biological triplicates. Data are expressed as the mean ± SD. Differences between two groups were determined by unpaired t-test. *P < 0.05.

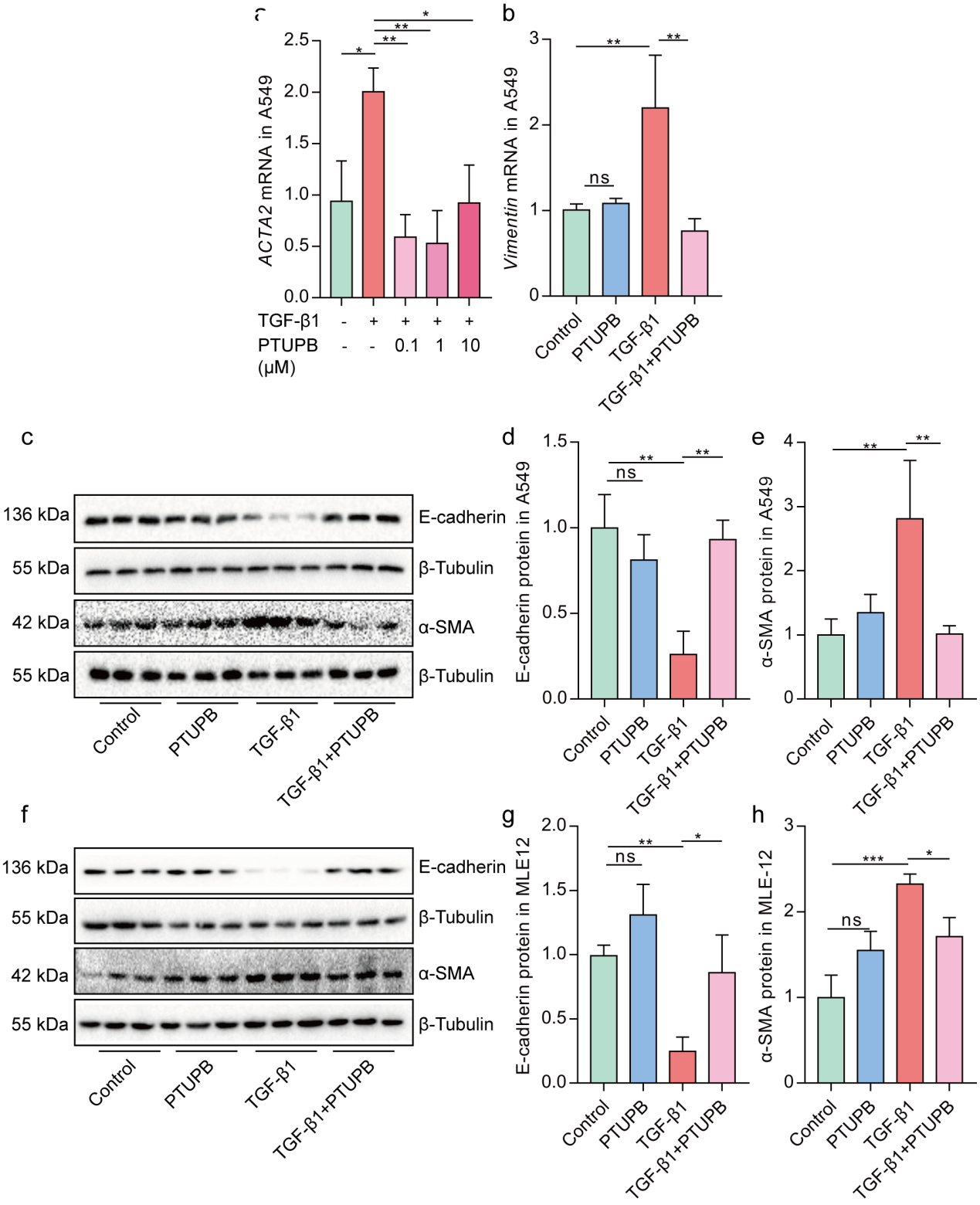


## Figure 3

**Prophylactic treatment of PTUPB suppresses the TGF-β1-induced EMT in A549 and MLE-12 cells.** Cells were treated with PTUPB (1 μM) for 1 h before the treatment with TGF-β1 (10 ng/mL). The mRNA expressions of *ACTA2* (a) and *Vimentin* (b) in A549 cells were detected by real-time PCR after TGF-β1 stimulation for 12 h (*n*=3). The protein expressions of E-Cadherin and α-SMA in A549 cells (c-e) and MLE12 cells (f-h) after TGF-β1 stimulation for 48 h were measured by western blotting (*n*=3). The data

shown are from a representative experiment with biological triplicates. Data are expressed as the mean ± SD. Differences among multiple groups were performed using ANOVA. Tukey's test was used as a post hoc test to make pairwise comparisons. * $P < 0.05$, ** $P < 0.01$ and *** $P < 0.001$.


## Figure 4

**Prophylactic treatment of PTUPB inhibits the migration induced by TGF-β1 in A549 cells.** Scratch wound healing assay showed that PTUPB (1 μM) inhibited the migratory ability of the A549 cells under the stimulation of TGF-β1 (10 ng/mL) (a-b, *n*=3, bar=500 px). PTUPB treatment didn't affect the proliferation of A549 under low-serum conditions (c, *n*=5). The data shown are from a representative experiment with biological triplicates. Data are expressed as the mean ± SD. Differences among multiple groups were performed using ANOVA. Tukey's test was used as a post hoc test to make pairwise comparisons. * $P < 0.05$ and ** $P < 0.01$.

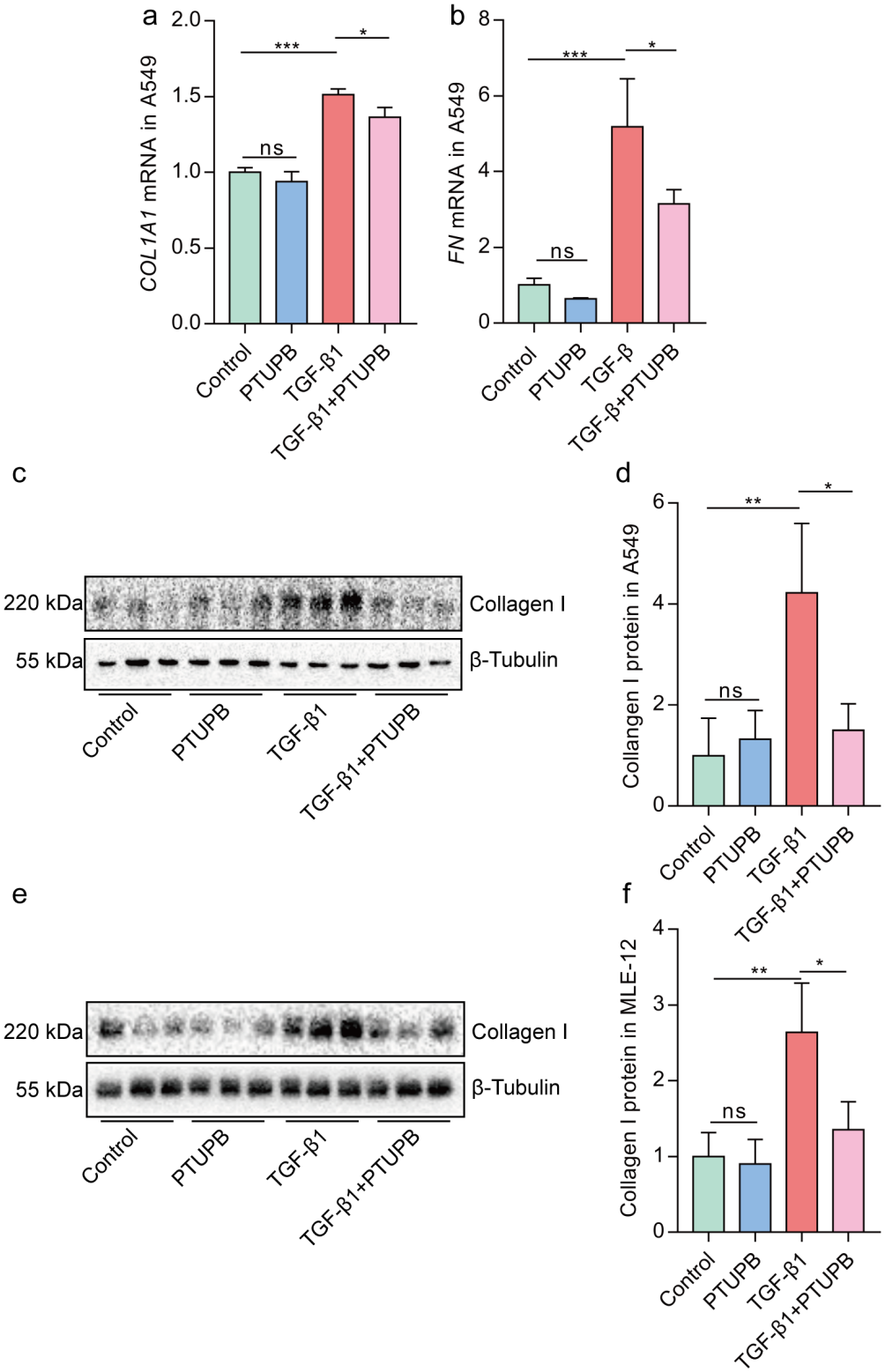


## Figure 5

**Prophylactic treatment of PTUPB inhibits the collagen synthesis induced by TGF-β1 in AECs.** Cells were treated with TGF-β1 (10 ng/mL) for 24 h present or absent the pre-treatment of PTUPB (1 μM) for 1 h. The mRNA expressions of *COL1A1* (a) and *FN* (b) in A549 cells were detected by real-time PCR (*n*=3). The protein expressions of Collagen I in A549 cells (c-d) and MLE-12 cells (e-f) were measured by western blotting after TGF-β1 stimulation for 48 h (*n*=3). The data shown are from a representative experiment

with biological triplicates. Data are expressed as the mean ± SD. Differences among multiple groups were performed using ANOVA. Tukey's test was used as a post hoc test to make pairwise comparisons. * $P < 0.05$, ** $P < 0.01$, and *** $P < 0.001$.


## Figure 6

**Prophylactic treatment of PTUPB disrupts the TGF-β1-Smad2/3 signaling pathway in AECs.** Cells were treated with PTUPB (1 μM) for 1 h before the treatment with TGF-β1 (10 ng/mL). Thirty Minutes after the TGF-β1 administration, the levels of p-Smad2 and p-Smad3 in A549 cells (a-c, *n*=3) and MLE12 cells (d-f, *n*=3) were detected by western blotting. Forty-eight hours after the TGF-β1 administration, the fluorescence intensity of Smad2 and Smad3 was detected by immunofluorescence (g, bar = 25 μm). Twelve hours after the TGF-β1 administration, the mRNA expressions of *ZEB1* and *SNAIL1* in A549 cells were detected by real-time PCR (h-i, *n*=3). The data shown are from a representative experiment with biological triplicates. Data are expressed as the mean ± SD. Differences among multiple groups were performed using ANOVA. Tukey's test was used as a post hoc test to make pairwise comparisons. * $P < 0.05$, ** $P < 0.01$, and *** $P < 0.001$.

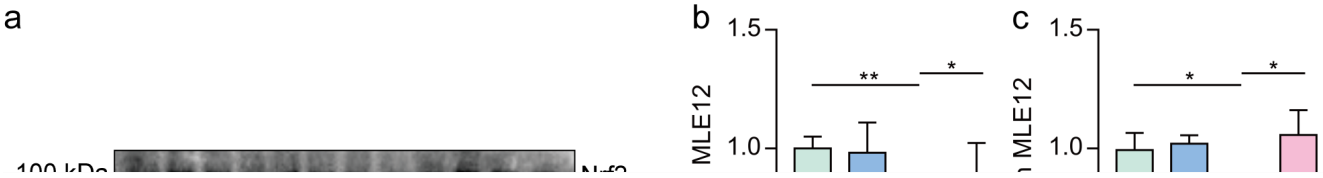


## Figure 7

**Prophylactic treatment of PTUPB restores Nrf2-dependent antioxidant pathways in TGF-β1-treated AECs.** Cells were treated with PTUPB (1 μM) for 1 h before the treatment with TGF-β1 (10 ng/mL). The protein expressions of Nrf2 and HO-1 in MLE12 cells (a-c) after TGF-β1 stimulation for 48 h were measured by western blotting (*n*=3). The ROS in MLE12 cells after TGF-β1 stimulation for 48 h were detected by a ROS kit (d, bar = 100 μm). The fluorescence intensity of Nrf2 was detected by immunofluorescence (d, bar = 25

μm). The data shown are from a representative experiment with biological triplicates. Data are expressed as the mean ± SD. Differences among multiple groups were performed using ANOVA. Tukey's test was used as a post hoc test to make pairwise comparisons. * *P < 0.05* and ** *P < 0.01*.

## Figure 8

**Inhibition of Nrf2 attenuates PTUPB regulation of TGF-β1/Smad signaling.** Cells were treated with PTUPB (1 μM) and ML385 (5 μM) for 1 h before the treatment with TGF-β1 (10 ng/mL). The protein expressions of Nrf2, HO-1, E-cadherin, and α-SMA in MLE12 cells (a-e) after TGF-β1 stimulation for 48 h were measured by western blotting (*n*=3). Twelve hours after the TGF-β1 administration, the mRNA expressions of *Zeb1* and *Snail1* in MLE12 cells were detected by real-time PCR (f-g, *n*=3). Forty-eight hours after the TGF-β1 administration, the fluorescence intensity of Smad2 and Smad3 was detected by immunofluorescence (h, bar = 50 μm). The data shown are from a representative experiment with biological triplicates. Data are expressed as the mean ± SD. Differences among multiple groups were performed using ANOVA. Tukey's test was used as a post hoc test to make pairwise comparisons. * *P* < 0.05, ** *P* < 0.01, and *** *P* < 0.001.

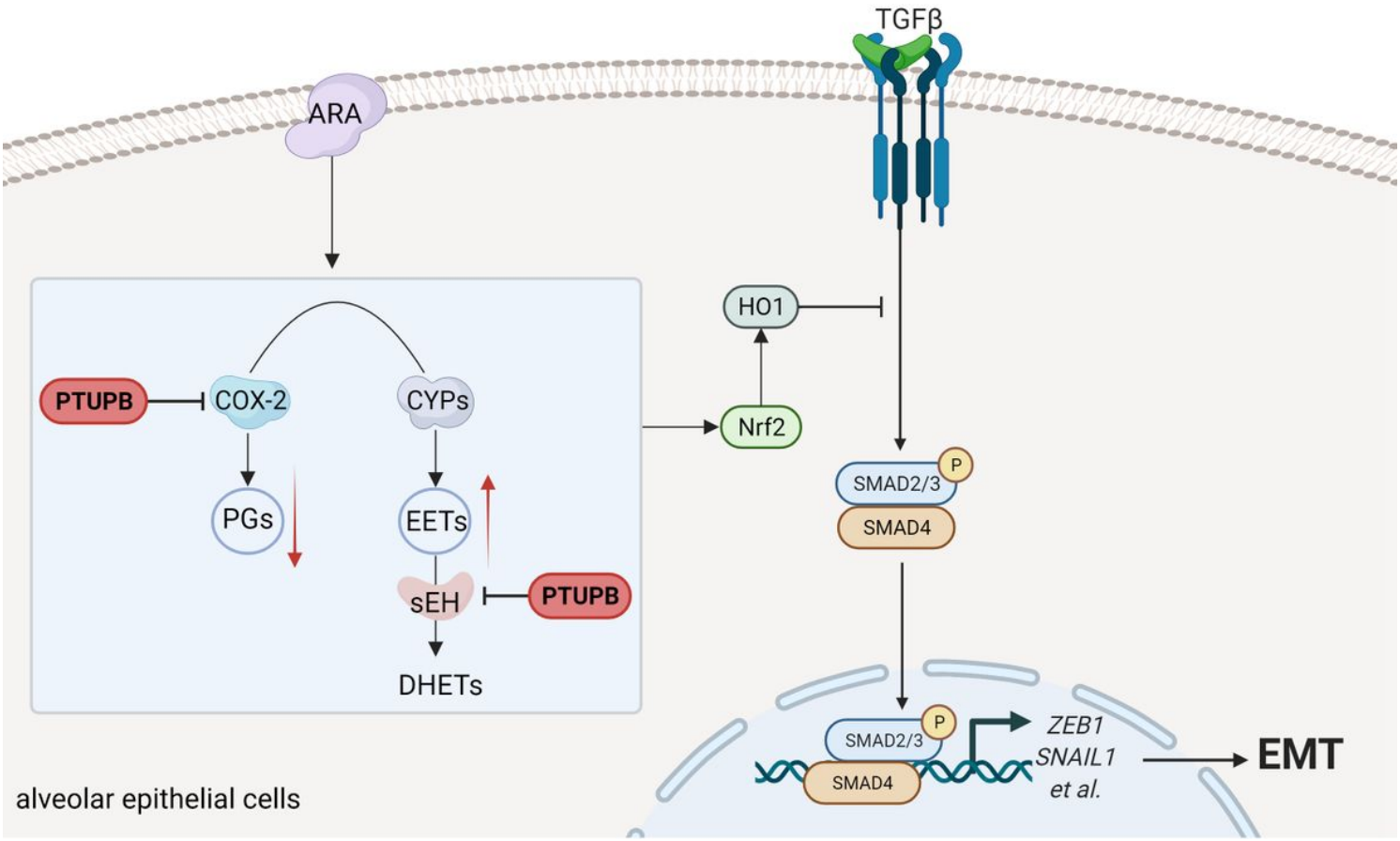


## Figure 9

**Schematic illustration.** A COX-2/sEH dual inhibitor PTUPB inhibits EMT induced by TGF-β1 in AECs.

# Supplementary Files

This is a list of supplementary files associated with this preprint. Click to download.

- Supplementarymaterials.docx